Korean J. Chem. Eng., 34(5), 1294-1304 (2017)
DOI: 10.1007/s11814-017-0066-5

pISSN: 0256-1115
eISSN: 1975-7220

REVIEW PAPER

Improved mechanical properties, barrier properties and degradation behavior of poly(butylenes adipate-co-terephthalate)/poly(propylene carbonate) films

Hongwei Pan*,,***, Yanping Hao*, Yan Zhao*,***, Xianzhong Lang*,***, Ye Zhang*,***, Zhe Wang***, Huiliang Zhang*,†, and Lisong Dong***

*Key Laboratory of Polymer Ecomaterials, Chinese Academy of Sciences, Changchun Institute of Applied Chemistry, Changchun 130022, China
**University of Chinese Academy of Sciences, Beijing 10080, China
***Engineering Research Center of Synthetic Resin and Special Fiber, Ministry of Education, Changchun University of Technology, Changchun 130022, China
(*Received 29 March 2016 • accepted 7 March 2017*)

Abstract—Poly(butylene adipate-co-terephthalate) (PBAT) was blended with poly(propylene carbonate) (PPC) by a twin screw extruder and then the blends were made onto films via the blown film technique. PPC dispersed uniformly in the PBAT matrix, and the glass transition temperature (T_g) of PBAT were decreased with the increasing content of PPC. Wide angle X-ray diffraction confirmed that the crystallite dimension of PBAT was decreased after blending PBAT with the amorphous PPC. The results of mechanical tests indicated that the PBAT/PPC films showed high tensile strength and tear strength. In addition, the PBAT/PPC films showed high carbon dioxide permeability and moderate oxygen and nitrogen permeability. After embedding in soil, the weight loss and mechanical properties analysis demonstrated that the films were remarkably biodegraded. These findings contributed to application of the biodegradable materials, such as design and manufacture polymer packaging.

Keywords: Poly(butylene adipate-co-terephthalate), Poly(propylene carbonate), Blown Films, Mechanical Properties, Biodegradable

INTRODUCTION

Biodegradable packaging materials, developed from natural products, has long been attractive due to the growing need for minimizing the deposition of nondegradable solid residues in the environment [1]. Natural polymers have wide sources, are environmentally safe and capable of biological degradation, so natural polymers could be deemed the first clinically used biodegradable biomaterials with economic and environmental benefits [2]. Considering the biodegradable character, natural polymers can be regarded as the first clinically used biodegradable biomaterials. Due to their natural abundance and low cost, many researchers have attempted to incorporate them into a great variety of plastic materials [3]. Poly (butylene adipate-*co*-terephthalate) (PBAT) resins are well known as biodegradable materials, which are aliphatic-aromatic copolyester and linear aliphatic thermoplastics. The chemical structure of PBAT is depicted in Scheme 1. In view of high toughness, good heat resistance, and high impact performance, blends of PBAT with other polymers, such as poly(lactic acid) (PLA) [4], thermoplastic starch (TPS) [5], polyhydroxy butyrate-*co*-valerate (PHBV) [6], polycaprolactone (PCL) [7], have been studied to modify the properties of polymers and expand their practical application. PBAT is also a flexible plastic designed for blow films. Further applications of these blends can be found in the food packaging field by improving their mechanical or barrier properties.

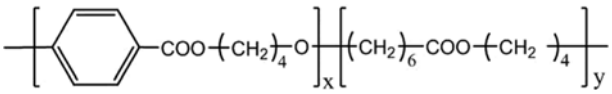

Scheme 1. Chemical structure of PBAT.

Poly(propylene carbonate) (PPC) is synthesized by the alternating copolymerization of propylene oxide with carbon dioxide [8-10]. Synthetic procedure and chemical structure of PPC are depicted in Scheme 2. PPC is a biodegradable aliphatic polycarbonate that can be degraded to H_2O and CO_2, and its synthesis can fix and recycle CO_2 in the environment. This cycle not only reduces the consumption of petroleum resource, but also decreases the massive emission of CO_2 [11,12]. It has found utilization in one-off packaging materials, dishware and board materials [13]. It is an amorphous polymer that exhibits superior tensile strength, high Young's modulus, and good degradability in surroundings of both boil and buffer solutions [14-16]. In addition, the amorphous nature

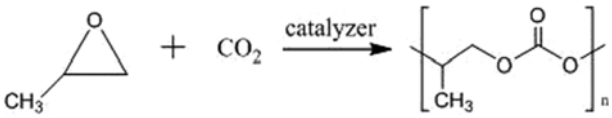

Scheme 2. Synthetic scheme and chemical structure of PPC.

†To whom correspondence should be addressed.
E-mail: hlzhang@ciac.jl.cn

of PPC can endow many unique properties, such as highly oxygen barrier property. Moreover, the carboxyl end-capped of PPC groups may easily cause special interactions with other components in blends, and its strong polar carbonate group may result in a transesterification reaction, improving the compatibility of blend systems [17]. PPC has been devoted to improving the mechanical properties of biodegradable blends, such as polylactide (PLA) [18], poly (butylene carbonate) (PBC) [19], poly(ethylene-co-vinyl alcohol) [20], poly(butylene succinate) (PBS) [21], and so on. In general, when the softer component forms a second phase in a more brittle continuous phase, it may act as a stress concentrator, which may enables ductile yield and prevents brittle failure. However, to produce PPC-based films, it is very important to improve its melt and static strength [22,23].

The biodegradation mechanism of the aliphatic-aromatic polyester is usually considered in both enzymatic and hydrolytic ways, of which the former is dominant when the polyester is buried in compost. These degradation processes may modify the structure and composition of PBAT, consequently, changing its thermal, crystallite dimension and mechanical properties [24-30]. Kijchavengkul et al. [31,32] found that the amorphous regions within PBAT were more susceptible than the crystalline regions. Wu et al. [33,34] studied the biodegradation behavior of PBAT and cellulose acetate composites in different mediums, and they found that the biodegradation rate of the composite was faster than that of the neat PBAT. Biodegradable behavior and properties of PBAT have been also reported by Zehetmeyer, Pawar, Muthuraj, and Mittal [35-38]. PPC was subjected to the influence of degradation agents such as oxygen, light, mechanical stress, temperature and water from which, separately or in combination during its life cycle (synthesis - processing - service life - discarding - recovery), arose chemical and physical changes that altered its stabilization mechanisms and long-term properties [39]. Many techniques have been used to individual study the degradation of PBAT and PPC, including scanning electron microscope (SEM), mechanical properties, weight loss, differential scanning calorimetry (DSC), and gel permeation chromatography (GPC), and so on.

However, to this day, the properties of PBAT/PPC films have not yet reported. The blending method remains the most popular modification technique in the preparation of film due to its simplicity and effectiveness in producing desired film properties [40]. The purpose of the present study was to investigate the miscibility, thermal, mechanical properties, gas barrier properties and biodegradability of the PBAT/PPC films.

EXPERIMENTAL

1. Materials

PBAT (Ecoflex FBX 1200), was supplied by BASF Corporation (Germany). PBAT (45% BA-co-55% BT) with a melt flow index of 3.3-6.6 g/10 min (at 190 °C, 2.16 Kg), density of 1.25-1.27 g/cm^3, the molecular weight of 1.42×10^5 g/mol, the glass transition temperature (T_g) of −29 °C, the melting point of 110-115 °C. PPC was supplied by Taizhou Bangfeng Plastic Co., Ltd. (China). The number average molecular weight (M_n) and polydispersity index (PDI) of the purified PPC were determined by GPC as 1.50×10^5 g/mol and 4.32, respectively.

2. Sample Preparation

Before blending, all polymers were dried in vacuum at 50 °C for 24 h. Blends of PBAT/PPC were prepared by melt mixing using a twin-screw extruder (SHJ-20, China). The mixing compositions of PBAT/PPC blends were 100/0, 90/10, 70/30, 50/50, and 0/100 w/w. The extrusion temperature was independently controlled at nine zones along the extruder barrel and strand die to achieve a temperature profile in the range of 155-170 °C. The resulting PBAT/PPC blends were pelletized in-line after being cooled in a water bath. The pellets were dried in an oven overnight at 45 °C.

Blends of PBAT/PPC were dried in vacuum at 40 °C overnight before blowing films. The PBAT/PPC films were blown using a 30.0 mm smooth-bore single-screw extruder, having an aspect ratio of 30 : 1 and fitted with a 46 mm diameter blown film die using external cooling air with temperature of 15 °C. The barrel temperature profile in different zones ranged from 160 to 175 °C and the screw speed was kept at 38 rpm. Moreover, the extruder output was 8 kg/h, the blowup ratio (BUR) was 6, the frost line height (distance from die exit) was 15 cm and the winding speed was 7.0 m/min. The thickness of the films was 30 μm.

3. Differential Scanning Calorimetry (DSC)

Thermal properties of the PBAT/PPC films were studied by differential scanning calorimeter (TA Instruments DSC Q20) with a universal analysis 2000 under nitrogen atmosphere. The weight of the samples was about 5-8 mg. The films were heated first from −60 to 180 °C at 10 °C/min (the first heating run) and held at 180 °C for 3 min to eliminate their previous thermal history. Following that, the samples were cooled to −60 °C and then heated to 180 °C again at 10 °C/min (the second heating run). The degree of crystallization of the samples is evaluated from the heat evolved during crystallization by the following relationship [Eq. (1)]:

$$x_c = \frac{\Delta H_f}{w_{PBAT}\times\Delta H_f^0}\times 100\% \quad (1)$$

where x_c is the degree of crystallinity of PBAT, ΔH_f is melting enthalpy of the PBAT in the blend, ΔH_f^0 is the melting enthalpy for 100% crystalline PBAT (114 J/g) [41] and w_{PBAT} is the weight fraction of PBAT in the blend.

4. Wide Angle X-ray Diffraction (WAXD)

Wide angle X-ray diffraction experiments of pure PBAT and PBAT/PPC blends were performed on a D8 advance X-ray diffractometer (Bruker, Germany) at room temperature in the range of 5-35° at a scanning rate of 4°/min. The Cu K_α radiation (λ=0.15418 nm) source was operated at 40 kV and 200 mA.

The apparent crystal size (ACS) was estimated by Scherrer's Eqs. (2) and (3) [42]:

$$ACS = \frac{K\lambda}{\beta_{hkl}\theta_{hkl}} \quad (2)$$

with

$$\beta = (B^2 - b^2)^{1/2} \quad (3)$$

where K, the Scherrer constant, takes a value of 0.9, λ is the wavelength of the X-ray (1.5406 Å) and θ is the Bragg angle. B is the half width in radians of the diffraction angle of the (011), (010),

(110), (100), and (111), and b is the instrumental constant (0.1°). The calculated values of ACS are listed in Table 5.

5. Thermal Stability

Thermogravimetric analysis (TGA) was performed using a Netzsch STA 409 PC (Germany) under a nitrogen protective atmosphere. All samples with weight of 10±0.2 mg were heated from 30 to 600 °C at 20 °C/min under nitrogen. The flow rate of nitrogen was set as 50 mL/min. The weight loss curves were of neat PBAT, neat PPC and PBAT/PPC (50/50) samples from dynamic measurements at heating rates of 5, 10, 20, and 30 °C/min.

The activation energy of decomposition, E, of the polymer can be calculated from the TGA curves by Eq. (4), which is referred to as Flynn-Wall-Ozawa method [43]:

$$\lg\beta = \lg\frac{AE}{RF(\partial)} - 2.315 - 0.457\frac{E}{RT} \quad (4)$$

where β is the heating rate, ∂ is the fractional conversion, $F(\partial)$ is the reaction mechanism function and has nothing to do with the temperature, E is the activation energy of decomposition, A is the pre-exponential factor, T is the absolute temperature and R is the gas constant.

6. Morphological Observation

The cryo-fractured surfaces of PBAT/PPC blends had undergone selective ethyl acetate removal of PPC component. The etching time was 15 min at room temperature. The cryo-fractured surfaces of PBAT/PPC blends were characterized by scanning electron microscopy (SEM) (model Japan JXA-840 ESEMFE). A layer of gold was sputter-coated uniformly over all the fractured surfaces before SEM observations.

7. Mechanical Properties Testing

Uniaxial tensile tests were carried out at 23±2 °C on an Instron 1121 testing machine (Canton MA). Specimens (20 mm×4 mm×0.03 mm) from the previously blown films were cut into a dumbbell shape in the machine direction (MD) and transverse direction (TD), respectively. The measurements were conducted at a cross-head speed of 20 mm/min at room temperature according to ASTM D882-2010. At least five runs for each sample were measured, and the results were averaged.

The right angle tearing strength was measured at 23±2 °C on an Instron 1121 testing machine (Canton MA). The measurements were conducted at a cross-head speed of 200 mm/min at room temperature according to QB/T 1130-91MD and TD, respectively. At least five runs for each sample were measured, and the results were averaged.

8. Barrier Properties

The permeability of oxygen (O_2), nitrogen (N_2), and carbon dioxide (CO_2) through film samples was measured using a Labthink VAC-V2 gas permeability tester with a manometric method in accordance with the GB 1038-1970 standard. The transmission rate was normalized with respect to the film thickness. The average of five measurements for each sample was reported.

Gas permeability measurements were performed using a constant-volume method at a feed pressure of 1 atm and a feed temperature of 20 °C. The diameter of the sample was 100 mm, thickness was 0.03 mm. The permeability was determined in the sequence O_2, N_2, and CO_2. The design of the permeation apparatus and the experimental procedure are described in detail elsewhere. The permeability coefficient of each gas was calculated by Eq. (5):

$$P_g = DS = 10^{10}\frac{V_d l}{ARTp_{up}}\left(\frac{dp}{dt}\right) \quad (5)$$

where P_g is the permeability coefficient of a film to gas in barrer (1 barrer=10^{-10} cm^3 [STP] cm cm^2 s^{-1} $cmHg^{-1}$), P_{up} is the upstream pressure (cmHg), dp/dt is the steady-state permeate-side pressure increase ($cmHgs^{-1}$), V_d is the calibrated permeate volume (cm^3), l is the film thickness (cm), A is the effective area of the film (cm), R is the universal gas constant (0.278 cm^3 cmHg cm^{-3} [STP] K^{-1}) and T is the absolute temperature (K). The apparent diffusion coefficient D (cm^2 s^{-1}) of the polymer film was calculated by $D=l^2/6\theta$, where θ is the time lag of the permeability measurement. The solubility coefficient S (cm^3 [STP] cm^{-3} $cmHg^{-1}$) was obtained from the relationship S=P/D.

9. Biodegradation in Soil

Method was adapted from the US standard ASTM D5988-96, which is a Standard Test method for determining aerobic biodegradation in soil of plastic materials. Samples measuring 100 mm×30 mm×0.03 mm were buried in boxes of alluvial-type soil that had been obtained from farmland top soil before planting in May 2015. The soil was sifted to remove large clumps and plant debris. Soil was maintained at approximately 35% moisture by weight, and the samples were buried at a depth of 10-15 cm. A control box consisted of only samples and no soil. The buried samples were dug out, washed in distilled water, dried in a vacuum oven at 35±2 °C for three days, and equilibrated in desiccators for at least one day.

The film weight before and after soil biodegradation test was recorded accordingly. The mechanical properties of the PBAT/MTPS films were conducted at a cross-head speed of 5 mm/min at room temperature according to ASTM D882-2010. At least five runs for each sample were measured, and the results were averaged. At the end of each month, one frame for each sample was retrieved, and the corresponding film samples were cleaned and dried at room temperature before characterization.

RESULTS AND DISCUSSION

1. Differential Scanning Calorimetry Investigation

Fig. 1(a), (b) depicts the DSC trace of samples. The variation trends of related parameters including the glass-transition temperature (T_g), melting enthalpy (ΔH_f) and crystallinity (X_c) of PBAT/PPC blends are presented in Table 1. As summarized there, with PPC content ranging from 0 to 50%, T_g of PBAT was decreased from −29.4 to −31.6 °C in the first heating run. In the PBAT/PPC blends, amorphous PPC could act as "solvent" [44]. Because of this solvent effect, the PPC molecule could permeate into the inside of PBAT molecule and decrease molecular stack density, the chain mobility was promoted as evidenced by the simultaneous decreasing of T_g, with increasing PPC content. However, the T_g of PPC was enhanced from 31.1 to 44.1 °C in the first heating run. It indicates that PBAT and PPC were incompatible. The T_g of the PPC in blends was increased, which might be due to free volume effect. From Table 1, it also showed that T_gs of PBAT and PPC component in the second heating run were changed smaller than those

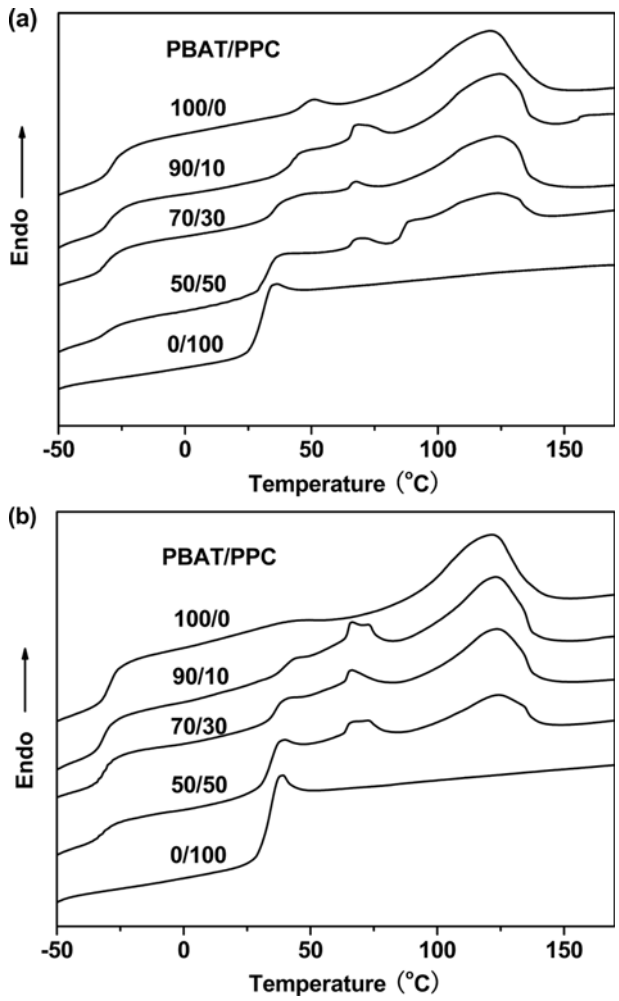

Fig. 1. DSC thermograms of the PBAT/PPC films: (a) in the first heating runs; (b) the second heating runs.

Table 1. Thermal properties of neat PBAT, neat PPC, and PBAT/PPC films

PBAT/PPC (w/w)	T_m (°C)	ΔH_f (J/g)	X_c (%)	$T_{g,PBAT}$ (°C)	$T_{g,PPC}$ (°C)
First heating run					
100/0	121.6	12.8	11.2	−29.4	--
90/10	123.2	11.2	10.9	−30.4	44.1
70/30	123.8	8.3	10.4	−30.8	36.2
50/50	124.4	5.7	10.0	−31.6	33.5
0/100	--	--	--	--	31.1
Second heating run					
100/0	121.3	13.4	11.7	−27.6	--
90/10	123.2	10.2	10.0	−30.3	41.2
70/30	123.6	6.8	8.5	−30.9	37.0
50/50	124.0	4.5	7.9	−31.5	34.5
0/100	--	--	--	--	33.4

in the first heating run. The main reason was that the samples had been eliminating their previous thermal history in the second heating run. As a statistically random copolyester, PBAT is composed of rigid butylene terephthalate (BT) units and the soft butylenes adipate (BA) units [45]. A small peak was observed around 65 °C obviously, which was the T_g of poly(butylene terephthalate) (PBT).

From Fig. 1(a), it was obvious that the melting temperature (T_m) of PBAT/PPC films was increased from 121.6 to 124.4 °C in the first heating run. The higher values of T_m indicated that PPC could contribute to an increase PBAT molecular chain mobility and have some intermolecular bonds exist between polymer chains. From Table 2, ΔH_f and X_c of PBAT/PPC films were much smaller than those of neat PBAT in the first and second heating runs. PPC could permeate into the amorphous region of PBAT, the crystallinity of PBAT was decreased.

Table 2. Crystallite dimension of the neat PBAT and PBAT/PPC blends

PBAT/PPC (w/w)	ACS (Å)				
	(011)	(010)	(110)	(100)	(111)
100/0	58.0	88.3	32.4	98.8	54.1
90/10	57.5	85.0	31.9	94.2	53.4
70/30	56.3	80.4	31.6	89.9	52.0
50/50	45.5	69.2	21.2	77.9	45.0
0/100	--	--	--	--	--

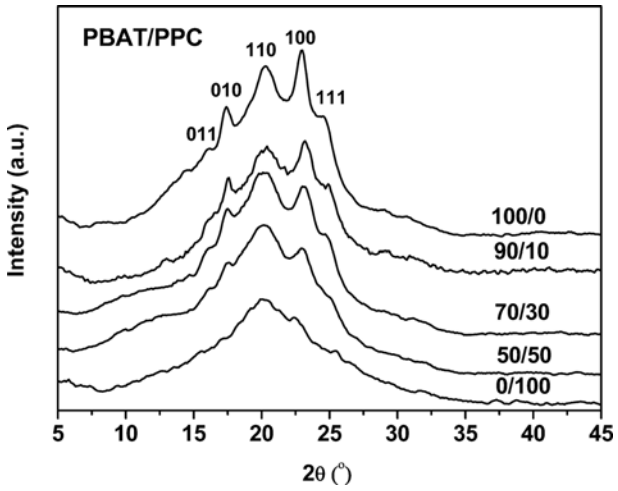

Fig. 2. X-ray diffraction patterns of neat PBAT, neat PPC, and PBAT/PPC films.

2. Wide Angle X-ray Diffraction (WAXD)

To investigate the crystallinity of films, the WAXD of neat PBAT, PPC, and PBAT/PPC films were recorded and shown in Fig. 2. The diffraction pattern of the neat PABT was characterized by five diffraction peaks at 2θ angle of 16.3°, 17.4°, 20.3°, 23.3°, and 25.1°, related to basal reflections (011), (010), (110), (100), and (111), respectively [46]. These peaks were also found with little deviation in Fig. 3.

The dispersion extent of PPC has typically been elucidated by WAXD, which allows a direct evidence of polymer chain intercalated into the PBAT. With increasing PPC content, it can be seen that the crystallite dimension of PBAT decreased within the blend

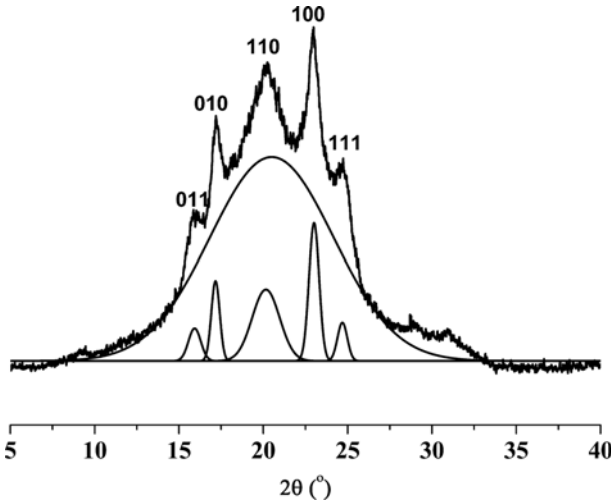

Fig. 3. Resolution of the WAXD curve of PBAT into the crystalline and amorphous portions.

films in Table 2. Intensity of the observed diffraction peaks was lower after added PPC, which was in agreement with the lower degree of crystallinity. Compared with PBAT, the intensity of diffraction peaks of PBAT/PPC films became weaker at (010), (100), and (111) refraction. The position of diffraction peaks had a small migration at 17.4°, 23.3°, and 25.1° obviously. Thus, it seems that the PPC likely hindered the crystal growth of PBAT. This indicates that melting PPC molecule chains were intercalated into amorphous area of PBAT successfully, which made the structure of crystal lattice more dispersible, the distances between crystal lattice were widened. In addition, entangled structures in amorphous area impeded the transportation of macromolecular chains between polymer chains, restricting the crystalline ability of PBAT and forming more amorphous phase [47]. Consequently, these results suggested that there was no important transcrystallinity at the PBAT/PPC interface; all peaks in the PBAT crystal structure were induced by PPC incorporation.

3. Thermal Stability of PBAT/PPC Films

The thermal stability of PBAT/PPC was monitored as a function of temperature. The thermogravimetric (TGA) curves and the derivative thermogravimetric (DTG) curves of neat PBAT, PPC, and the PBAT/PPC blends are shown in Fig. 4.

The thermal degradation process of PBAT/PPC blends had two stages in the temperature range of 100-350 °C and 350-500 °C in the Fig. 4(a). The first stage (100-350 °C) and the second stage (350-500 °C) might attribute to the degradation of PPC component and PBAT component, respectively. PPC obeyed a two-step pyrolysis mechanism: 100-250 °C, an unzipping by "back biting"; 250-350 °C, main-chain random scission [48,49]. PBAT also showed two obvious decomposition stages: 250-380 °C, the beginning of chain scission; 380-500 °C, aromatization reaction. It was found that the $T_{5\%}$ of neat PBAT was at 366 °C, while the $T_{5\%}$ of thermal decomposition of PBAT/PPC blends was sharply lower than that of neat PBAT. It indicates that the incorporation of PPC into PBAT reduced the thermal stability of PBAT/PPC blends.

By comparing the DTG curves of PBAT/PPC blends with those

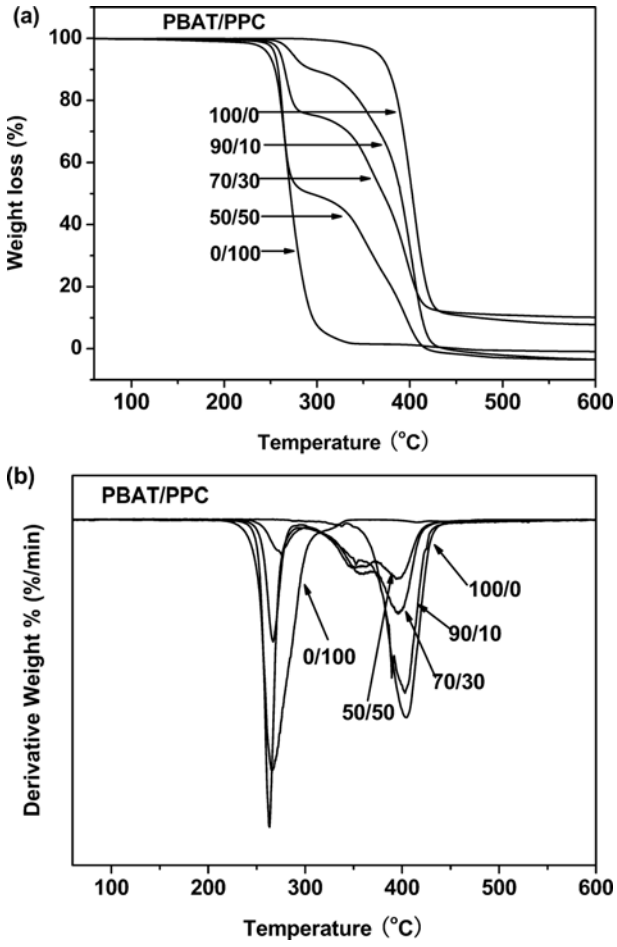

Fig. 4. (a) TGA; (b) DTG curves of neat PBAT, neat PPC, and PBAT/PPC films.

of neat PBAT and PPC, it can be seen that the profile of curves for PBAT/PPC blends was not a simple merge of the curves. The DTG curve of neat PBAT showed two stages in the Fig. 4(b). PBAT is a copolymer, which consists of poly(butylene terephthalate) (PBT) and poly(butylene adipate) (PBA) macromolecular chains. The first stage in the range of 286-385 °C, loss of mass (20%) was attributed to a loss of PBA. The second stage in the range of 385-430 °C, loss of mass (68%) was attributed to thermal degradation of PBT. For neat PPC, an intense decomposition stage was observed with peak temperature at 266.8 °C. In the PBAT/PPC blends, the decomposition peak of PBAT shifted from 404.7 to 394.1 °C. The maximum degradation temperature of PBAT was higher about 130 °C than neat PPC. PPC could be easily thermal degradation [50]; therefore, the thermal stability of the PBAT/PPC blends decreased with increasing PPC content.

Fig. 5 shows lines of $\lg\beta$ versus $1000\times0.457/8.314/T$ for all the neat PBAT, neat PPC and PBAT/PPC (50/50) samples. It can be seen that these lines have a good linear relationship. From Table 3, when the weight loss was 5% the values of E of PBAT/PPC (125.7 kJ/mol) were higher than that of PPC (119.5 kJ/mol), which might be attributed to the lower initial decomposition temperature of PPC. Because higher decomposition temperature means stronger interaction within polymer chains, which results in an increase of

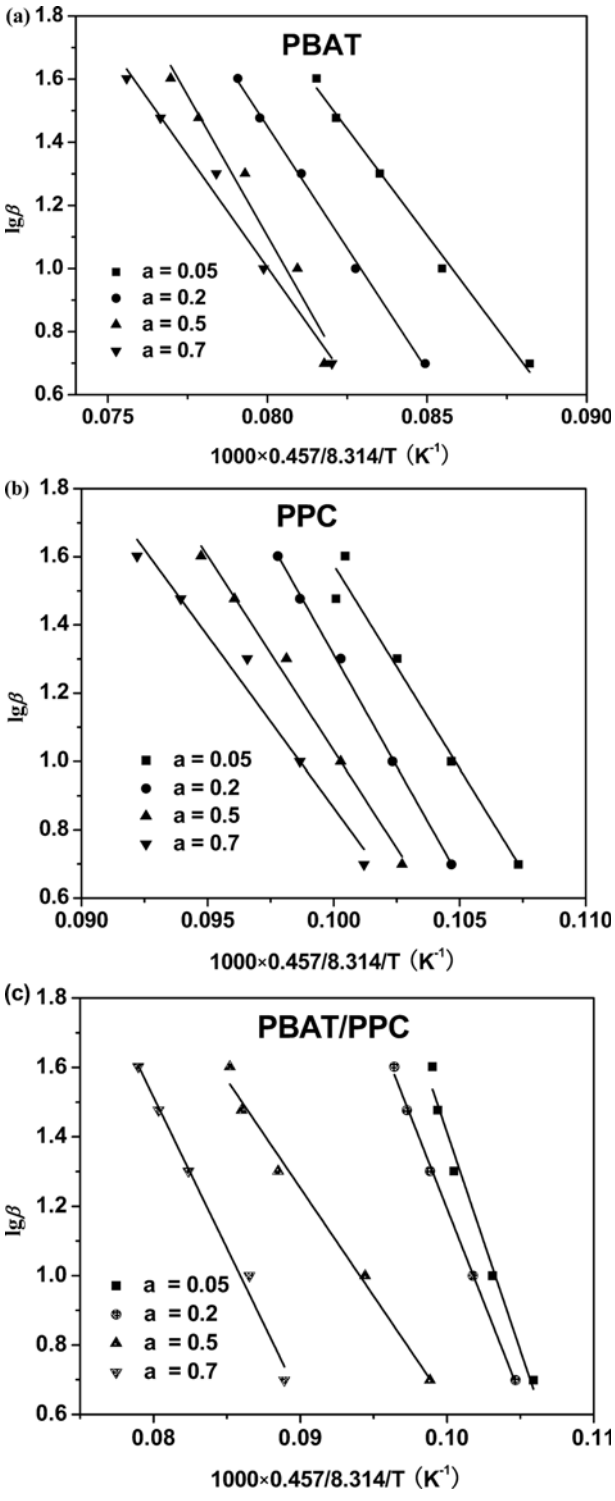

Fig. 5. Flynn-Wall-Ozama plots at the following different weight loss: (a) neat PBAT; (b) neat PPC; (c) PBAT/PPC 50/50.

activation energy. Regarding the other thermal degradation kinetic parameters, the average value of $\overline{E}$ was 152.4 kJ/mol for the PBAT, while a value of 116.1 kJ/mol for the PPC. In the following thermal degradation stage, the $\overline{E}$ of PBAT/PPC was apparently much lower than that neat PBAT and PPC, which could be ascribed to the much low compatibility of PBAT/PPC blends.

Table 3. Activation energies of neat PBAT, neat PPC, and PBAT/PPC (50/50) blend determined by Flynn-Wall-Ozawa method

Conversion ∂	PBAT E (kJ/mol)	PPC E (kJ/mol)	PBAT/PPC (50/50) E (kJ/mol)
0.05	134.8	119.5	125.7
0.2	154.3	131.1	107.5
0.5	178.1	114.1	62.3
0.7	142.5	100.7	87.0
	Average value of activation energies $\overline{E}$ (kJ/mol)		
	152.4	116.1	95.6

4. Morphology Analysis

It is well recognized that the properties of a polymer blend are strongly influenced by its morphology. Fig. 6 presents the scanning electron microscope (SEM) micrographs of cryo-fractured surfaces of PBAT/PPC blends. PPC could be etched by ethyl acetate. It can be seen that the black pores must be formed by the removal of PPC in the fracture surface.

As shown in Fig. 6(a), the surface of virgin PBAT was smooth and featureless. When the content of the PPC was 10 wt% [Fig. 6(b)], the pores were small and the diameter of the pore was inhomogeneous in PBAT. The pore in the PBAT became bigger with increasing PPC content up to 30 wt% [Fig. 6(c)]. Interestingly, when PPC content increased to 50 wt% [Fig. 6(d)], the pores became interconnected, which indicated the formation of the co-continuous phase. The above experimental results clearly demonstrated the influence of blend ratio on the phase structure of PBAT/PPC blends. When PPC content was less than 50 wt%, PBAT crystals filled the whole film sample and PPC dispersed in it. When the PPC content reached 50%, the formation of the co-continuous phase between PBAT and PPC could be increasing the influence of PPC, leading to a high content of amorphous material.

5. Mechanical Properties

The mechanical properties of PBAT/PPC films were different in the machine direction (MD) and transverse direction (TD) sections. The tensile strength and elongation at break of the PBAT/PPC blend films are plotted in Fig. 7. It can be seen that the tensile strength and elongation at break in MD were much higher than that in TD. This could be attributed to the orientation of molecular chains along MD. The values of Young's modulus and tear strength of virgin PBAT and PBAT/PPC films are presented in Table 4.

From Fig. 7, PBAT showed predominant elongation at break, which was exceptionally high, about 731% (MD) and 632% (TD); however, it had a poor tensile strength and low Young's modulus. PPC had a tensile strength of about 40 MPa (MD) and 38 MPa (TD) at room temperature, but was poor in flexibility, leading to early break. Wu et al. also reported that neat PPC was very rigid and brittle with tensile strength around 38 MPa [19]. The addition of PPC component changed the tensile behavior of the PBAT films significantly. It is obvious that 30 wt% of PPC was an optimum content of improving the mechanical properties of PBAT/PPC blends in this work. The tensile strength was successfully increased to 41 MPa (MD) and 39 MPa (TD) of 70/30 PBAT/PPC sample, while the elongations at break gradually decreased to

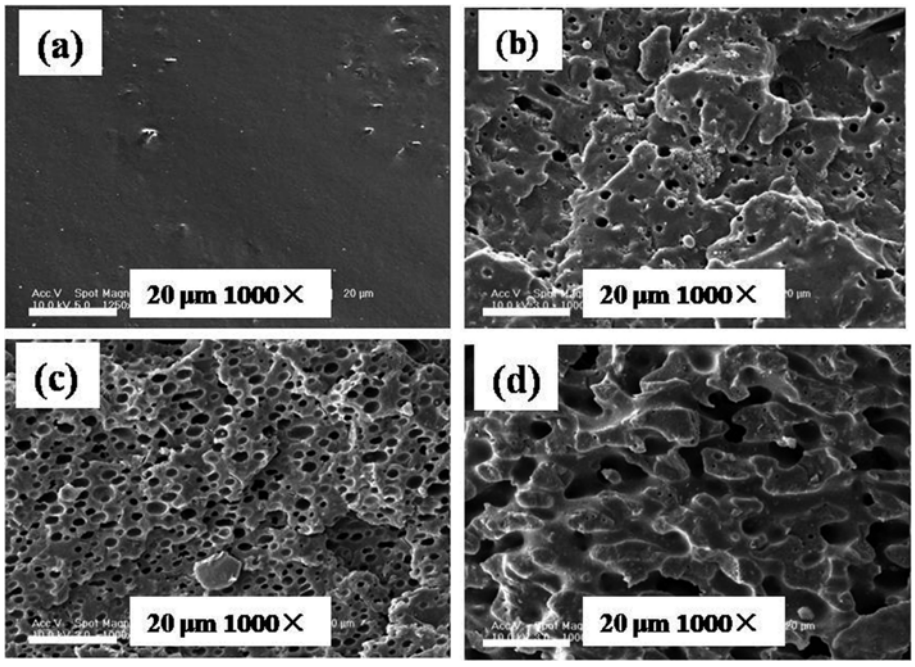

Fig. 6. SEM micrographs of the cryo-fractured surfaces of PBAT/PPC blends: (a) 100/0; (b) 90/10; (c) 70/30; (d) 50/50.

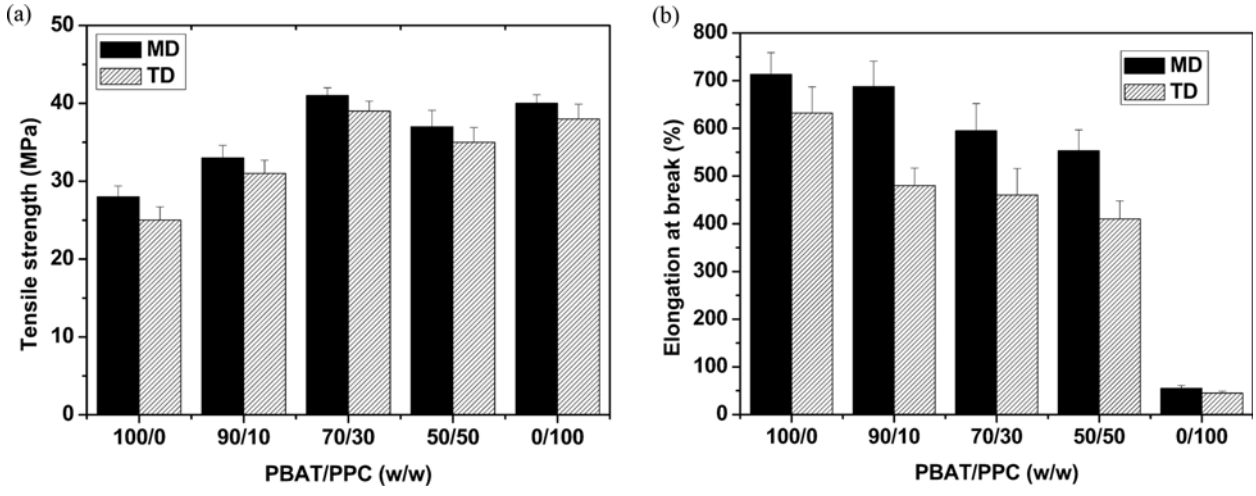

Fig. 7. Tensile behavior of PBAT/PPC films: (a) Tensile strength; (b) Elongation at break.

Table 4. Mechanical properties of PBAT/PPC blend films

PBAT/PPC (w/w)	100/0	90/10	70/30	50/50	0/100
Young's modulus MD/TD (MPa)	110±12/68±10	181±14/90±9	351±22/130±15	590±27/420±26	2640±43/2480±33
Tear strength MD/TD (kN/m)	101±5/124±3	111±7/127±7	125±5/137±7	134±3/153±7	175±3/166±6

595% (MD) and 460% (TD). The improvement in mechanical properties was associated with the interactions between two polymers, as well as the effective distribution of the dispersion phase. The phase inversion of the two-phase system had occurred and the mechanical properties began to decrease when the PPC component changed from 30 to 50 wt%. This might be attributed to the formation of co-continuous phase morphology. The continuous PPC phase resulted in a lower tensile strength, which required less energy to break the materials.

Young's modulus of polymer blends mainly depends on the modulus of each constitutive component and blend composition. It is also somewhat affected by the interactions and changes in the

phase morphology. From Table 4, neat PBAT film exhibited modulus about 110 MPa (MD) and 68 MPa (TD) and neat PPC film exhibited modulus about 2,640 MPa (MD) and 2,480 MPa (TD), respectively. When the PPC content was up to 50 wt%, the modulus was increased to 590 MPa (MD) and 420 MPa (TD). Young's modulus is the ratio between the stress and the applied deformation, which also mainly depended on the chemical bond forces and the interaction between macromolecules. Therefore, Young's modulus for the blends exhibited a significant increase in higher loading of PPC, similar to the change of the tensile strength.

The results of the tear strength on the film specimens are shown in Table 4. The neat PBAT specimen exhibited relatively low tear strength values of 101 kN/m (MD) and 124 kN/m (TD). In contrast, the tear strength of PBAT/PPC films revealed a substantial increase as the PPC content increased. From above discussion, the 50/50 PBAT/PPC film could achieve a comprehensive application, such as tensile strength, elongation at break, and tear strength.

6. Barrier Properties

The barrier effect of polymer films was evaluated and quantified by measuring the gas permeability coefficients (P_g), which indicated the amount of gas that permeated per unit of area and time. A lower P_g means a better barrier effect. All the polymers, especially to the food packing materials, have been proven to be relatively permeable to small molecules. It is often needed to avoid or at least decrease the transfer of gases such as oxygen, carbon dioxide and water vapor between the contents of the package and the surrounding environment [51]. Therefore, barrier films must pre-

Table 5. Permeability coefficient (P_g) of oxygen, nitrogen and carbon dioxide through the neat PBAT, PPC, and PBAT/PPC films

PBAT/PPC (w/w)	Permeabilities (barrer)s (20 °C, 1 atm)		
	P_g (O_2)	P_g (N_2)	P_g (CO_2)
100/0	0.73±0.012	0.59±0.021	7.12±0.18
90/10	0.55±0.037	0.31±0.034	5.13±0.25
70/30	0.29±0.004	0.011±0.0016	4.22±0.19
50/50	0.17±0.028	0.087±0.0007	2.61±0.15
0/100	0.13±0.019	0.0097±0.0008	1.43±0.05

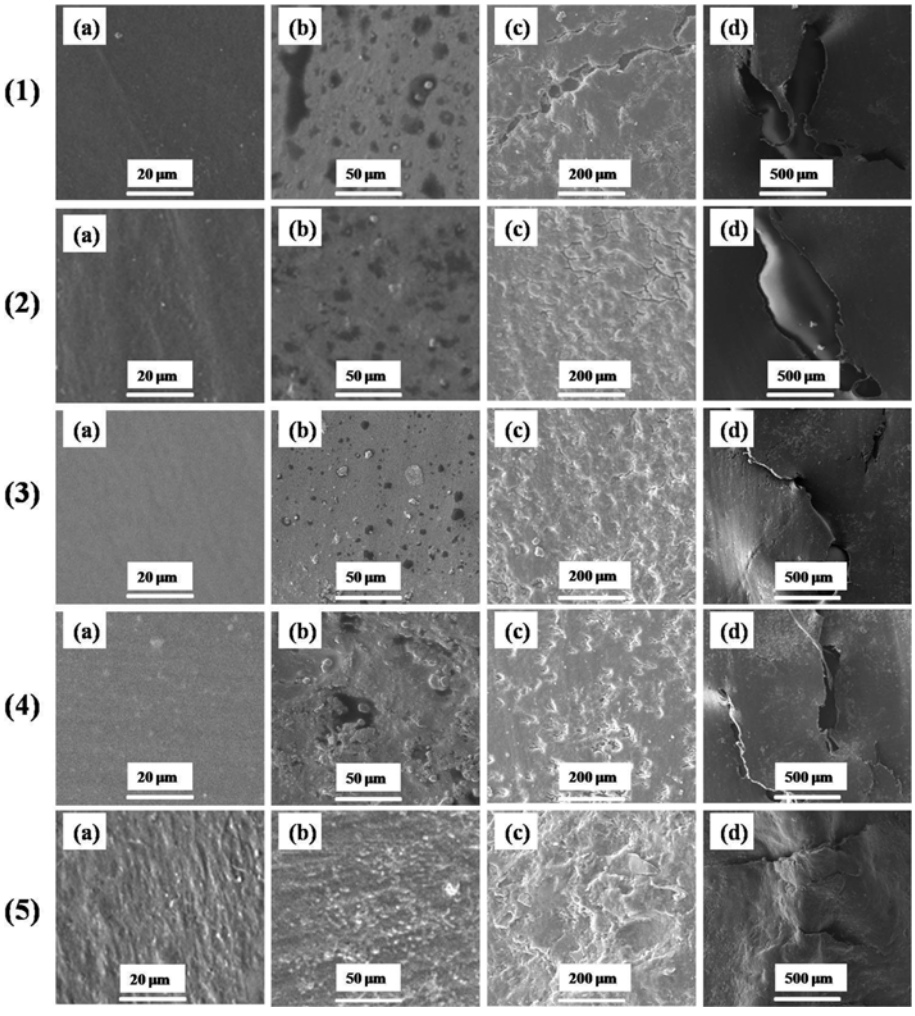

Fig. 8. SEM micrographs of the morphology of PBAT/PPC films degradation for different time in soil. Biodegradation times: (a) 0 days; (b) 30 days; (c) 60 days; (d) 120 days. PBAT/PPC (w/w): (1) 100/0; (2) 90/10; (3) 70/30; (4) 50/50; (5) 0/100.

vent or at least decrease the gas transfer between the product and the surrounding atmosphere.

The gas permeation properties of the PBAT/PPC films were measured at 20 °C and 1 atm. The P_g values of the oxygen (O_2), nitrogen (N_2) and carbon dioxide (CO_2) of the film samples are shown in Table 5. The order of gas permeability tested in the study was $CO_2>O_2>N_2$, which was typically in the reversed order of their respective kinetic diameter. P_g (CO_2) (7.12 to 2.61 barrers) of PBAT/PPC films was ten-times higher than those of oxygen and nitrogen, when the PPC content was increased from 0 to 50 wt%. The decrease in CO_2 permeability coefficient was more responsible for the increase in gas barrier property because the occupancy of the number of active sites was increased with the increased PPC present in the polymer matrix. Barrier properties of materials are highly dependent on both their chemical and morphological structure [52,53]. PPC is synthesized by the alternating copolymerization of propylene oxide with carbon dioxide. Therefore, carbon dioxide has better PPC solubility than oxygen and nitrogen in the PBAT/PPC films. PPC has excellent flexible and ductility, its molecule chains can intercalate into amorphous area of PBAT; the factor is based on the constriction in movement of molecules in polymeric chains due to the chemical interaction between PBAT and PPC. Since the presence of oxygen is a key factor in facilitating thermal degradation [54], the barrier effect of oxygen determines the final thermal stability of film. When the PPC content was up to 50 wt%, the oxygen and nitrogen permeability values decreased from 0.73 and 0.59 barrers to 0.17 and 0.087 barrers, respectively. The main reason was that less availability of the number of active sites was found in PPC matrix for physical interaction with oxygen and nitrogen molecules. According to the values of the barrier effect of oxygen, nitrogen and carbon dioxide, we concluded that the 50/50 PBAT/PPC film had an excellent barrier properties, where the minimum value of permeability coefficient was reached. It might be the existence of either the bond (-o-) in both PBAT and PPC molecular structure or the more flexible of PPC, which increased the interaction between the PBAT and PPC interface, thus reducing permeability.

7. Degradation of PBAT/PPC Films

The method of soil burial degradation was used to study biodegradability of PBAT/PPC film material. The photographs of the remaining samples of films were obtained from scanning electron microscope with different degradation periods and shown in Fig. 8. From Fig. 8(a), the unburied specimens had smooth surfaces. The samples began to biodegrade for 30 days [Fig. 8(b)], black spots were observed on the film surface of neat PBAT film. After biodegradation for 60 days, large fissures were observed on the PBAT film surface. Kijchavengkul et al. [55] reported that PBAT would be degraded without leaving any residue in the compost soil a few weeks. As shown in Fig. 8(5, a), the surface of neat PPC film had only minor corrosion. After biodegradation for 60 days, the PPC film surface was severely corroded in Fig. 8(5, c). The main reason might be that PPC was amorphous copolymer. The amorphous regions in a semi-crystalline biodegradable polyester are usually more susceptible to microorganisms and enzymes than the crystalline regions. The less compact structures would eventually facilitate the biodegradation and hydrolysis of the amorphous regions prior to the crystalline regions [56-58]. It indicates that the PBAT/PPC films degraded faster with increasing the PPC content. After 120 days biodegradation [Fig. 8(d)], the sample showed a greater extent of degradation with some larger and wider cracks on every film surface, which might be ascribed to the reduced compatibility between PBAT and PPC matrix.

Table 6. Weight loss of neat PBAT, neat PPC, and PBAT/PPC as a function of incubation time in soil

PBAT/PPC (w/w)	30 days (g)	60 days (g)	120 days (g)
100/0	0.002	0.027	0.035
90/10	0.005	0.031	0.039
70/30	0.007	0.024	0.041
50/50	0.010	0.030	0.047
0/100	0.018	0.039	0.059

The original weight of sample was 0.16 g

The weight loss and tensile strength of the PBAT/PPC films were measured after different degradation times. Table 6 shows the weight loss changed as a function of time for the PBAT/PPC films buried in the soil. The degree of weight loss increased with prolonged time. Kim et al. [59] reported that PPC was biodegradable in mice by surface erosion, which might probably result from enzymatic hydrolysis and oxidative degradation processes. They also reported that there were numerous pits and holes on the surface of PPC at 60 days, and this phenomenon was more obvious at 120 days, indicating a high degree of degradation of the PPC film. From Table 6, the original weight of sample films was 0.16 g. With increasing PPC content, weight loss of samples was increased over the first 60 days. After 120 days, the 100/0, 90/10, 70/30, 50/50, and 0/100 PBAT/PPC exhibited a weight loss of approximately 21.8%, 24.4%, 25.6%, 29.3%, and 36.9%, respectively. It indicates that the PBAT/PPC films could be remarkably degraded in the soil.

The tensile strength and elongation at break are shown in Fig. 9. The tensile strength of 100/0, 90/10, 70/30, 50/50, and 0/100 PBAT/PPC films was 28.3, 35.2, 38.8, 42.2, and 40.6 MPa before biodeg-

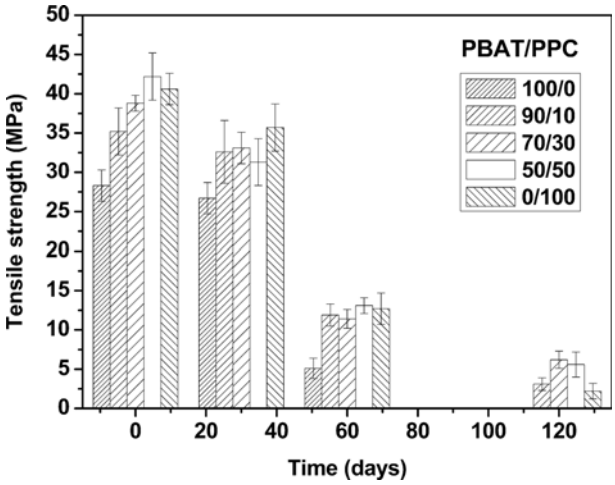

Fig. 9. Tensile strength of neat PBAT, neat PPC, and PBAT/PPC films as a function of incubation in soil.

radation test, respectively. After biodegradation for 30 days, the tensile strength of films samples was 26.7, 32.6, 33.1, 31.3, and 35.7 MPa. There was an obvious decrease for all of the film samples after biodegradation. The PBAT/PPC films showed slightly higher degradation value than the neat PBAT and PPC. As discussed in the SEM analysis, cavities and cracks started to appear during the second month as the result of microorganism activities. The higher degradation rate for the blends might be attributed to the cocontinuous phase morphology of PBAT/PPC blends. The huge number of defects resulted in numerous of corrosion points, which gave rise to the deteriorated tensile strength. During biodegradation for 60 days and 120 days, the tensile strength for all of the PBAT/PPC films decreased about 0-6 MPa, but it was nearly invariable for the neat PBAT. These films with interconnected fissure were biodegradable, biocompatible and innocuous [60], which would be appropriate for biodegradable packaging engineering.

CONCLUSIONS

Thermal properties, crystal behavior, mechanical and barrier properties of PBAT/PPC films were investigated. Compared with pure PBAT, the glass transition temperature (T_g) and thermal degradation temperature ($T_{5\%}$) were gradually decreased with increasing PPC content. PPC component of the blends was amorphous in the blown films, which resulted in a smaller crystallite dimension of PBAT/PPC films. The tensile strength as well as the tear strength of PBAT/PPC films were improved significantly compared with that of neat PBAT. The tear strength increased from 101 kN/m (MD) and 124 kN/m (TD) of neat PBAT to 175 kN/m (MD) and 166 kN/m (MD) of the 50/50 PBAT/PPC film. The incorporation of PPC component substantially increased the gas barrier properties of PBAT/PPC films. The weight loss data proved that PBAT was still biodegradable in the presence of PPC. From this research, novelty biodegradable films can be obtained, which are suitable for packaging application.

ACKNOWLEDGEMENT

This work was supported by the fund of Science & Technology Bureau of Changchun City of China (No. 2013279), Chinese Science Academy (Changchun Branch) (No. 2014SYHZ0019), Development and Reform Commission of Jilin Province of China (2015Y027), and the National Science Foundation of China (No. 51021003).

REFERENCES

1. O. V. Lopez, N. E. Zaritzky, M. V. E. Grossmann and M. A. Garcia, *J. Food Eng.*, **116**, 286 (2013).
2. X. H. Li and S. D. Deng, *Korean J. Chem. Eng.*, **32**, 2347 (2015).
3. L. S. Nair and C. T. Laurencin, *Polym. Sci.*, **32**, 762 (2007).
4. L. Jiang, M. P. Wolcott and J. W. Zhang, *Biomacromolecules*, **7**, 199 (2006).
5. R. P. H. Brandelero, F. Yamashita and M. V. E. Grossmann, *Carbohyd. Polym.*, **82**, 1102 (2010).
6. P. Russo., B. Vetrano, D. Acierno and M. Mauro, *Polym. Compos.*, **9**, 1461 (2012).
7. Y. W. Di, S. Iannace, E. D. Maio and L. Nicolais, *J. Polym. Sci. Part B: Polym. Phys.*, **41**, 670 (2003).
8. S. Inoue, H. Koinuma and T. Tsuruta, *J. Polym. Sci. Part B: Polym. Lett.*, **7**, 287 (1969).
9. S. Inoue, H. Koinuma and T. Tsuruta, *Makromol. Chem.*, **130**, 210 (1969).
10. L. J. Chen, Y. S. Qin, X. H. Wang, Y. S. Li, X. J. Zhao and F. S. Wang, *Polym. Int.*, **60**, 1697 (2011).
11. N. Wang, X. X. Zhang, J. G. Yu and J. M. Fang, *Polym. Int.*, **57**, 1027 (2008).
12. J. Tao, C. J. Song, M. F. Cao, D. Hu, L. Liu and N. Liu, *Polym. Degrad. Stab.*, **94**, 575 (2009).
13. S. S. Zeng, S. J. Wang, M. Xiao, D. M. Han and Y. Z. Meng, *Carbohyd. Polym.*, **86**, 1260 (2011).
14. S. J. Wang, S. C. Tjong, L. C. Du, X. S. Zhao and Y. Z. Meng, *J. Appl. Polym. Sci.*, **85**, 2327 (2002).
15. Q. Zhu, Y. Z. Meng, S. C. Tjong, X. S. Zhao and Y. L. Chen, *Polym. Int.*, **51**, 1079 (2002).
16. Y. Z. Meng, L. C. Du, S. C. Tjong, Q. Zhu and A. S. Hay, *J. Polym. Sci. Part A: Polym. Chem.*, **40**, 3579 (2002).
17. J. Li, M. F. Lai and J. J. Liu, *J. Appl. Polym. Sci.*, **98**, 1427 (2005).
18. X. F. Ma, J. G. Yu and N. Wang, *J. Polym. Sci B: Polym. Phys.*, **44**, 94 (2006).
19. D. D. Wu, W. Li, Y. Zhao, Y. J. Deng, H. L. Zhang and H. X. Zhang, *Chinese J. Polym. Sci.*, **33**, 444 (2015).
20. X. L. Wang, F. G. Du, J. Jiao, Y. Z. Meng and R. K. Y. Li, *J. Biomed. Mater. Res. Part B: Appl. Biomater.*, **83**, 373 (2007).
21. H. L. Zhang, X. H. Sun, Q. Y. Chen, M. Q. Ren, Z. H. Zhang, H. F. Zhang and Z. S. Mo, *Chinese J. Polym. Sci.*, **25**, 589 (2007).
22. W. F. Chen, M. Z. Pang, M. Xiao, S. J. Wang, L. S. Wen and Y. Z. Meng, *J. Reinf. Plast. Comp.*, **29**, 1545 (2010).
23. X. H. Li, Y. Z. Meng, S. J. Wang, A. V. Rajulu and S. C. Tjong, *J. Polym. Sci. Pol. Phys.*, **42**, 666 (2004).
24. M. Day and D. M. Wiles, *J. Appl. Polym. Sci.*, **16**, 191 (1972).
25. N. Torres, J. J. Robin and B. Boutevin, *Euro. Polym. J.*, **36**, 2075 (2000).
26. R. J. Ehrig, *Plastics Recycling: Products and Processes*, Hanser Publishers, New York (1992).
27. L. Reigh and S. Stivala, *Elements of Polymer Degradation*, McGraw-Hill, New York (1971).
28. X. Colin and J. Verdu, *Comptes. Rendus. Chimie.*, **9**, 1380 (2006).
29. M. A. Spinace and M. A. De Paoli, *J. Appl. Polym. Sci.*, **80**, 20 (2001).
30. S. Karlsson, *Adv. Polym. Sci.*, **169**, 201 (2004).
31. T. Kijchavengkul, R. Auras, M. Rubino, E. Alvarado, J. R. C. Montero and J. M. Rosales, *Polym. Degrad. Stab.*, **95**, 99 (2010).
32. T. Kijchavengkul, R. Auras, M. Rubino, S. Selke, M. Ngouajio and R. T. Fernandez, *Polym. Degrad. Stab.*, **95**, 2641 (2010).
33. C. S. Wu, *Carbohyd. Polym.*, **87**, 1249 (2012).
34. C. S. Wu, *Polym. Degrad. Stab.*, **97**, 2388 (2012).
35. G. Zehetmeyer, S. M. M. Meira and J. M. Scheibel, *J. Appl. Polym. Sci.*, **133**, 43212 (2016).
36. S. P. Pawar, A. Misra and S. Bose, *Colloid. Polym. Sci.*, **293**, 2921 (2015).
37. R. Muthuraj, M. Misra and A. K. Mohanty, *J. Appl. Polym. Sci.*, **132**, 42189 (2015).

38. V. Mittal, A. U. Chaudhry and N. B. Matsko, *J. Appl. Polym. Sci.*, **131**, 40816 (2014).
39. U. Witt, T. Einig, M. Yamamoto, I. Kleeberg, W. D. Deckwer and R. J. Muller, *Chemosphere*, **44**, 289 (2001).
40. N. A. M. Nazri, W. J. Lau and A. F. Ismail, *Korean J. Chem. Eng.*, **32**, 1853 (2015).
41. S. Ravati, C. Beaulieu, A. M. Zolali and B. D. Favis, *AIChE J.*, **60**, 3005 (2014).
42. M. Kakudo and N. Kasai, *X-Ray Diffraction by Polymers*, Kodansha Press, Tokyo (1972).
43. T. Ozawa, *Bull. Chem. Soc. Jpn.*, **38**, 1881 (1965).
44. M. Gao, Z. J. Ren, S. K. Yan, J. R. Sun and X. S. Chen, *J. Phys. Chem. B.*, **116**, 9832 (2012).
45. K. Kuwabara, Z. Gan, T. Nakamura, H. Abe and Y. Doi, *Biomacromolecules*, **3**, 390 (2002).
46. F. Chivrac, Z. Kadlecova, E. Pollet and L. Averous, *J. Polym. Environ.*, **14**, 393 (2006).
47. Y. Zhao, Y. Zhang, Z. L. Li, H. W. Pan, Q. L. Dong and L. J. Han, *Korean J. Chem. Eng.*, **33**, 1104 (2016).
48. B. Liu, L. Chen, M. Zhang and A. Yu, *Macromol. Rapid. Commun.*, **23**, 881(2002).
49. J. K. Varghese, S. J. Na, J. H. Park, D. Woo, I. Yang and B. Y. Lee, *Polym. Degrad. Stab.*, **95**, 1039 (2010).
50. Y. P. Hao, H. L. Yang and H. L. Zhang, *Polym. Degrad. Stab.*, **128**, 286 (2016).
51. X. F. Ma, J. G. Yu and A. Zhao, *Compos. Sci. Technol.*, **66**, 2360 (2006).
52. J. Seo and H. Han, *Polym. Degrad. Stab.*, **77**, 477 (2002).
53. L. Li, M. J. Liu and S. Li, *Polymer*, **45**, 2837 (2004).
54. X. Wen, K. Y. Zhang, Y. Wang, L. J. Han, C. Y. Han and H. L. Zhang, *Polym. Int.*, **60**, 202 (2011).
55. T. Kijchavengkul, R. Auras, M. Rubino, M. Ngouajio and R. T. Fernandez, *Chemosphere*, **71**, 942 (2008).
56. M. Mochizuki and M. Hirami, *Polym. Adv. Technol.*, **8**, 203 (1997).
57. Z. H. Gan, K. Kuwabara, H. Abe, T. Iwata and Doi Y., *Polym. Degrad. Stab.*, **87**, 191 (2005).
58. G. Kale, R. Auras and S. P. Singh, *Packag. Technol. Sci.*, **20**, 49 (2007).
59. G. Kim, M. Ree, H. Kim, I. J. Kim, J. R. Kim and J. I. Lee, *Macromol. Res.*, **16**, 473 (2008).
60. D. D. Ju, L. J. Han, J. J. Bian, Z. Q. Guo, F. Li and S. Chen, *RSC. Adv.*, **5**, 5474 (2015).